Available online at www.sciencedirect.com
ScienceDirect
Planetary and Space Science 55 (2007) 1103–1112
Planetary and Space Science
www.elsevier.com/locate/pss

Middle atmosphere polar warmings on Mars: Simulations and study on the validation with sub-millimeter observations

Paul Hartogh*, Alexander S. Medvedev, Christopher Jarchow

Max Planck Institute for Solar System Research, Katlenburg-Lindau D-37191, Germany

Accepted 4 July 2006
Available online 26 January 2007

Abstract

Temperature inversions and the warmings over the winter poles in the Martian atmosphere occur due to the adiabatic heating associated with the downward branch of the Hadley circulation. We present results of simulations with a recently developed GCM which suggest that the warmings are the manifestations of the global meridional transport, and are strongly related to atmospheric eddies (planetary waves and tides). To date, sets of data required for the validation of the predicted warmings and the corresponding circulation patterns do not extend far enough into the middle atmosphere of Mars. This motivated our radiative and retrieval simulations to demonstrate that sub-millimeter observations can provide the required fields to validate and constrain the GCM results.

Keywords: Martian atmosphere; General circulation; Polar warming; Sub-millimeter wave remote sensing; Temperature and wind retrieval

1. Introduction

The global circulation of the Martian atmosphere became a focus of extensive studies over the last decade. Great amounts of vertical temperature samplings covering the planet's atmosphere from pole to pole with good horizontal resolution at different seasons have been obtained from the Thermal Emission Spectrometer onboard the Mars Global Surveyor (MGS–TES) (e.g., Smith et al., 2001), and is being collected from the Planetary Fourier Spectrometer onboard the European Mars Express (e.g., Formisano et al., 2005). These observations are supported by numerical simulations using the ever increasing number of general circulation models (GCMs) of the Martian atmosphere (e.g., Haberle et al., 1993; Hourdin et al., 1995; Wilson and Hamilton, 1996; Forget et al., 1999; Kuroda et al., 2005; Moudden and McConnel, 2005; Hartogh et al., 2005).

One particular interesting aspect of the Martian atmosphere circulation are temperature inversions and the associated warmings in the middle atmosphere over the winter poles. These features have been observed during both northern (e.g., Theodore et al., 1993; Santee and Crisp, 1993) and southern winters (e.g., Deming et al., 1986). They are believed to be caused by the adiabatic heating due to the downward branch of the transport cell over the poles (Wilson, 1997). Earlier numerical experiments with Martian GCMs failed to reproduce strong winter polar warmings. Partially, this inability was explained by insufficiently high upper lids of the model domains which inhibited a full development of the Hadley circulation (Barnes and Haberle, 1996). Later, it was shown that a strong northern winter polar warming can be simulated with an increased amount of dust corresponding to dust storm conditions (Wilson, 1997). He demonstrated that the enhanced aerosol heating expands the Hadley circulation poleward, and, therefore, intensifies downward motions over the pole.

Inversions of the zonal mean temperature over the winter poles occur in the terrestrial atmosphere during both solstices. The location of the winter polar temperature maximums on Earth approximately coincides with the stratopause, however their origin is not related to the increased absorption of the

*Corresponding author.
E-mail addresses: hartogh@mps.mpg.de (P. Hartogh), medvedev@mps.mpg.de (A.S. Medvedev), jarchow@mps.mpg.de (C. Jarchow).

0032-0633/$ - see front matter © 2007 Elsevier Ltd. All rights reserved.
doi:10.1016/j.pss.2006.11.018

solar radiation by ozone since there is no sun in the winter high latitudes. Similarly, even an increased dust load cannot result in the direct diabatic heating over the winter poles on Mars. Apparently, the adiabatic heating associated with the downward motions is the main reason for the winter polar temperature inversions on both planets. Thus, winter polar warmings are the manifestation of the global meridional circulation in the middle atmosphere of Mars. The cross-equatorial transport in the terrestrial middle atmosphere is induced primarily by the breaking planetary and gravity waves (Andrews et al., 1987). This so-called "extra-tropical pump" mechanism can exist in the Martian atmosphere as well. Barnes (1990) and Collins et al. (1997) studied the sensitivity of the meridional circulation in the Martian atmosphere to the forcing by breaking gravity waves. Using a GCM, Barnes and Hollingsworth (1987) explored a potential causation of sudden polar warmings by planetary waves. Hartogh et al. (2005) noticed a strong sensitivity of the polar temperature to the variations in the large-scale eddy forcing. They demonstrated that the meridional circulation is driven primarily by eddies during the dustless northern summer solstice (aerocentric longitude $L_s = 90^\circ$), at least below 70 km and outside the tropics.

The nature of the solstitial transport, and the related mechanism of winter polar warmings is still not fully understood. The outstanding questions are: what are the relative roles of the diabatic and adiabatic heating? What kind of waves controls the temperature inversions? What are the implications to the global atmospheric transport on Mars? Despite the great amount of Martian GCM simulations towards studying this mechanism, a lack of observational data does not allow its usable validation. The winter polar temperature maxima on Mars usually occur above $\approx$ 50 km, while the infrared (IR) spectrometers on the Martian orbit (e.g., TES and PFS) can retrieve atmospheric temperature only from below $\approx$ 60 km in limb measurements. The paucity of the data and the observational errors do not permit to reliably constrain the numerical models in the middle atmosphere. Even the magnitude and location of the warmings are still poorly known.

Temperature and wind profiles have been provided by ground-based mm and sub-mm observations up to $\approx$ 80 km. The disadvantage of these measurements, however, is the limited spatial resolution of ground-based sub-millimeter telescopes. In most cases, they provide disk averaged temperatures; at best (during Martian oppositions) they resolve the Martian disk with several points. This will change dramatically with the availability of new interferometers, especially the Atacama Large Millimeter Array (ALMA), since the new instruments will resolve the Martian disk with fractions of an arc-second. Another approach to determine upper atmospheric winds and temperature is the microwave limb sounding technique. It has been successfully applied in the Earth atmospheric science since early nineties, e.g., the Microwave Limb Sounder on the Upper Atmosphere Research Satellite, and the Microwave Atmospheric Sounder on the ATLAS 1 to 3 missions.

In this paper, we present some results of polar warming simulations with a recently developed Martian GCM (Hartogh et al., 2005) along with the discussion of the global meridional circulation. Performing radiative transfer and retrieval simulations, we demonstrate that the data obtained with ground-based and satellite-borne sub-millimeter instruments can provide the required fields to validate and constrain our GCM results. The outline of this paper is as follows. In Section 2, some results of simulations with the Martian GCM are shown, and a short discussion of parameters which are required to constrain the model is provided. The ground-based and limb sounding microwave approaches are discussed in Section 3. Section 4 presents the retrieval simulations for a sub-millimeter wave limb sounder.

2. Martian GCM results

To illustrate the relation of the winter polar warmings with the global meridional circulation, we present some results of simulations with a Martian GCM. This model has been described in detail by Hartogh et al. (2005). The current version has the resolution $11.25^\circ \times 5^\circ$ in longitude and latitude, respectively, $\approx$ 1 km in vertical, and covers the atmosphere from the surface to about 120 km. The model physics includes a comprehensive set of physical parameterizations relevant to the Martian conditions: non-LTE CO_2 radiation scheme, gravity wave drag, dust radiation, turbulent diffusion, and surface energy budget parameterizations. The model employs the realistic topography derived from the Mars Orbiter Laser Altimeter measurements (Delacourt et al., 2003), surface albedo map (Christensen et al., 2001), and the thermal inertia distribution at the surface (Mellon et al., 2000).

Fig. 1a presents a snapshot of the zonally averaged temperature simulated at the southern winter solstice, $L_s = 90^\circ$ for the low-dust condition. This scenario includes a uniformly distributed dust below 60 km with the nominal visible optical depth 0.2. The temperature maximum of about 190 K is seen over the Southern pole between 60 and 70 km. This peak cannot occur as the direct result of the solar radiation absorption by either CO_2 or dust because the winter pole is not illuminated by the Sun. The reason for this temperature inversion is purely dynamical: it appears due to the adiabatic heating associated with the air sinking over the pole. White stream lines in Fig. 1a display the calculated residual circulation with the strong downward motions over the winter pole. The descending flux is the part of the cross-equatorial Hadley cell. Therefore, the magnitude of the downward vertical velocity (and, consequently, the adiabatic heating) depends on the strength of the entire circulation pattern.

The mechanism of the meridional circulation forcing can be quantified if one uses the mean zonal momentum equation in the Transformed Eulerian Mean (TEM) formulation (Andrews et al., 1987, Eq. 3.5.5). Neglecting the transience of the atmospheric fields for seasonal means

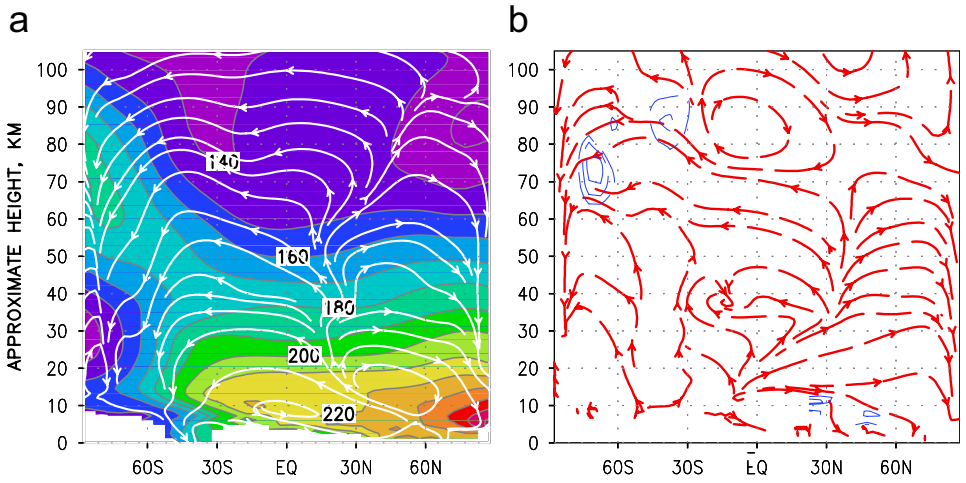

Fig. 1. Results of the simulation with the Martian GCM for $L_s = 90°$: (a) zonal mean temperature (shaded), and the residual circulation (white stream lines); (b) Eliassen–Palm fluxes (red arrows) and their divergence (thin blue lines).

and in mid- to high latitudes, this equation takes the form

$$\bar{v}^* \approx -(f\rho_0)^{-1}\nabla \cdot \mathbf{F}. \quad (1)$$

In (1), $\bar{v}^*$ is the South–North meridional velocity, ρ_0 is the mean density, $f = 2\Omega \sin\phi$ is the Coriolis parameter, Ω is the rotational frequency of the planet, ϕ is the latitude. In the right-hand part, $\mathbf{F} = (0, -\rho_0\overline{v'u'}, \rho_0 f\overline{v'\theta'}/\bar{\theta}_z)$ is the Eliassen–Palm (EP) flux, or the flux of wave action. Overbars in (1) denote longitudinal averagings, while the primed quantities represent deviations from zonal means, or eddies. The above equation illustrates the so-called "extra-tropical pump" described by Plumb (2002) for the terrestrial atmosphere. It is seen that the meridional circulation in mid- to high latitudes is forced primarily by the eddies (planetary and gravity waves, tides). The calculated **F** are plotted in Fig. 1b with the red arrows. It is seen, that the waves originate mainly near the surface (by the flow over the uneven topography) or in the warm summer hemisphere where the diurnal variations in the solar radiation absorption by the surface, atmospheric CO_2 and dust excite solar tides. The wave action carried by these planetary waves and tides propagates horizontally and vertically in accordance with the refractive properties of the atmosphere, as shown in Fig. 1b. The convergence and divergence of the EP fluxes (plotted with the thin blue lines in Fig. 1b) provide the poleward forcing for the air, as indicated in (1). The strong downward flow over the winter pole in our simulation is the result of the enhanced EP flux divergence seen in Fig. 1b.

The magnitude and location of the simulated polar temperature maximum in Fig. 1a is highly sensitive to the parameters of the model: resolution, sponge layer near the top of the model, use of the LTE or non-LTE radiation scheme, surface parameters, dust scenario. To constrain GCMs, measurements of both the wind and temperature from the ground to well above 60–70 km are required. Zonally averaged wind and temperature can provide a direct validation for the strength and location of the polar warmings, while the deviations of the local fields from their zonally averaged values (primed quantities in the definition of the EP fluxes) can shed a light on the details of the circulation forcing. Future theoretical and observational progress on the Martian middle atmosphere will require simultaneous wind and temperature measurements. In particular, the correlation $\overline{v'T'}$ can be used to determine both the residual transport velocities and the Eliassen–Palm fluxes. Typical observed (Lellouch et al., 1991) and simulated winds in this part of the atmosphere have magnitudes of several tens or even hundreds of $m\,s^{-1}$. Even zonally averaged meridional velocities reach several tens of $m\,s^{-1}$, about an order of magnitude stronger than on Earth. In the simulation shown in Fig. 1, the meridional velocity, $\bar{v}$, varies from -30 to $15\,m\,s^{-1}$ above 50 km. This suggests that wind measurements with even a moderate accuracy ($\pm 10\,m\,s^{-1}$) can provide usable constraints for Martian GCMs.

To date, the most extensive climatology of the Martian temperature exists for layers below 40 km. It was derived from the MGS–TES nadir measurements (Smith et al., 2001). Similar temperature retrievals from the Planetary Fourier Spectrometer (PFS) onboard the European Mars Express Mission will increase the data base for the lower atmosphere of Mars. Limb measurements from both instruments can provide additional information about the temperature up to 60 km, however with higher errors (Smith et al., 2001). In the next section, we will discuss the potential capability of ground-based mm and sub-mm observations, and present the simulations of a sub-mm limb sounding experiment dedicated for Mars.

3. Sounding Martian upper atmospheric temperatures and winds in the microwave range

3.1. Ground-based observations

In general, the carbon monoxide rotational transitions have been used to monitor the temperature of the Martian

atmosphere. The 1–0 transition in the atmosphere of Mars has been detected for the first time by Kakar et al. (1977). Assuming a constant vertical profile of CO, vertical profiles of temperature have been retrieved. Clancy et al. (1990) analyzed the temperature variations of the Martian atmosphere derived from ground-based millimeter wave observations between 1975 and 1989. Lellouch et al. (1991) presented for the first time Martian middle atmospheric Doppler winds derived from CO 2–1 single dish (IRAM 30 m) observations. Moreno et al. (2001) reported about interferometric observations of Martian winds around 50 km altitude with five times better spatial resolution. With the technological progress and the availability of better observation sites, higher (including 4-3) transitions have been measured. Fig. 2 shows an example of a vertical profile we derived from the observations of the 3–2 line at 345 GHz at the Sub-Millimeter Telescope (SMT) in Arizona in March 1997. Generally, the upper altitude limit of Martian atmospheric temperature and wind observations increases with the CO line strength. It depends on the disk averaged temperature profile which, in turn, is related to the solar longitude, i.e., the distance of Mars from the Sun. During southern summers, the solar flux is larger, and the disk averaged temperatures are higher than during northern summers. This lifts the altitude of a given pressure level and the upper altitude limit of the retrieval by several km compared to northern summers. For the calculations below we use northern summer disk averaged temperature profiles as the worst case scenario.

According to our calculations, the maximum of the line centre weighting function appears around 1 Pa (~60 km) for the CO 1–0 rotational transition, and at about 0.1 Pa (~4 km) for CO 3–2 (cf. Clancy and Sandor, 1998). For the 5–4 and higher transitions, the line centre weighting function appears around 0.04 Pa (~80 km) which defines the (worst case) upper height limit for nadir observations of wind and temperature in the mm and sub-mm range. Taking into account the atmospheric transmission (see Fig. 3), we conclude that the 6–5 transition of CO (see weighting functions in Fig. 4) is the best candidate for ground-based temperature and wind observations in the altitude range required for the validation of our model results. This is because the median of the 225 GHz opacity statistics at the ALMA site is around 0.05 with lowest opacities during the southern winter of 0.025 (Radford and Nyman, 2001). The longest baselines of ALMA may provide spatial resolutions sufficient to resolve the Martian atmospheric limb. Since the line of sight in a limb is much longer than in the nadir geometry, and the atmosphere is vertically resolved by the interferometer fringes, the information about the wind and temperature up to 100 km and higher can, in principle, be gained. However, for reasonable integration times these measurements will suffer from a poor signal to noise ratios (SNR), especially for upper atmospheric observations requiring high spectral resolution, and we doubt that this kind of observations could constrain our model calculations.

3.2. Observations from an orbiting satellite

From our point of view, the best approach for obtaining the required fields would be a limb sounder on a low polar orbit around Mars. As mentioned above, the limb sounding concept has the advantage of a longer line of sight compared to nadir observations: in the optical thin case, the observable air mass is up to a factor 50 larger. Nadir observations require a very accurate knowledge of the detected molecular line shape (i.e., a high SNR), since vertical information is related to the pressure broadening and the opacity of the line. Scanning the limb provides additional geometrical information through the knowledge of the pointing (tangential) height. This relaxes the requirement on SNR and increases the measurements efficiency. For a detailed description of microwave limb sounding see for instance (Waters, 1993).

Since the early 1990s, limb sounding microwave instruments have been successfully applied for the investigation of the Earth middle atmosphere dynamics and chemistry (e.g., Waters et al., 1995; Aellig et al., 1996). A millimeter wave limb sounder for the Cassini mission, orbiting Titan

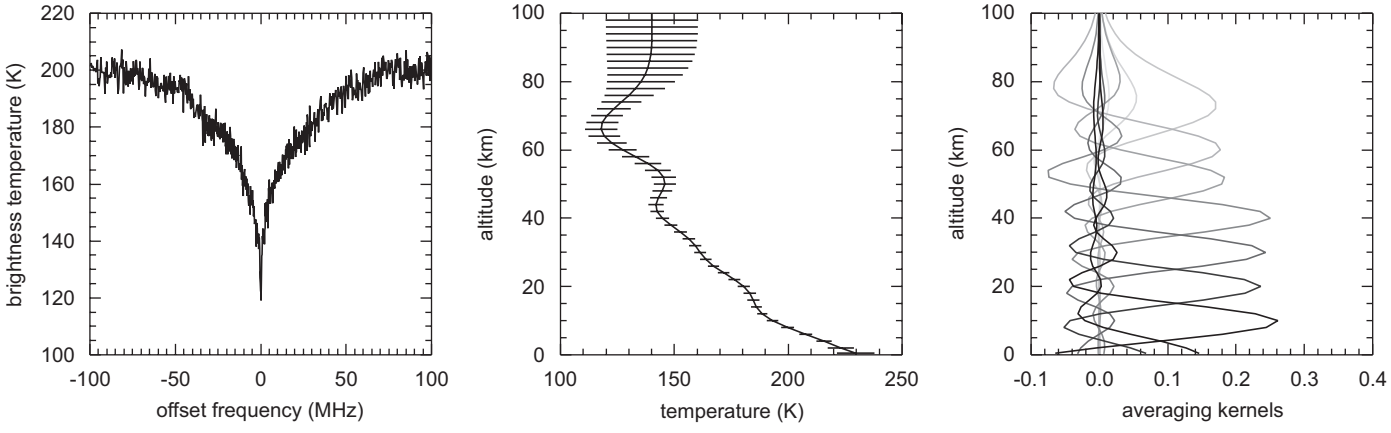

Fig. 2. CO 3-2 spectrum of Mars, observed with the Sub-Millimeter Telescope (SMT) on Mt. Graham, Arizona in March 1997, and the retrieved vertical distribution of the temperature. The averaging kernels show that the sensitivity of the retrieval decreases substantially above 70 to 75 km.

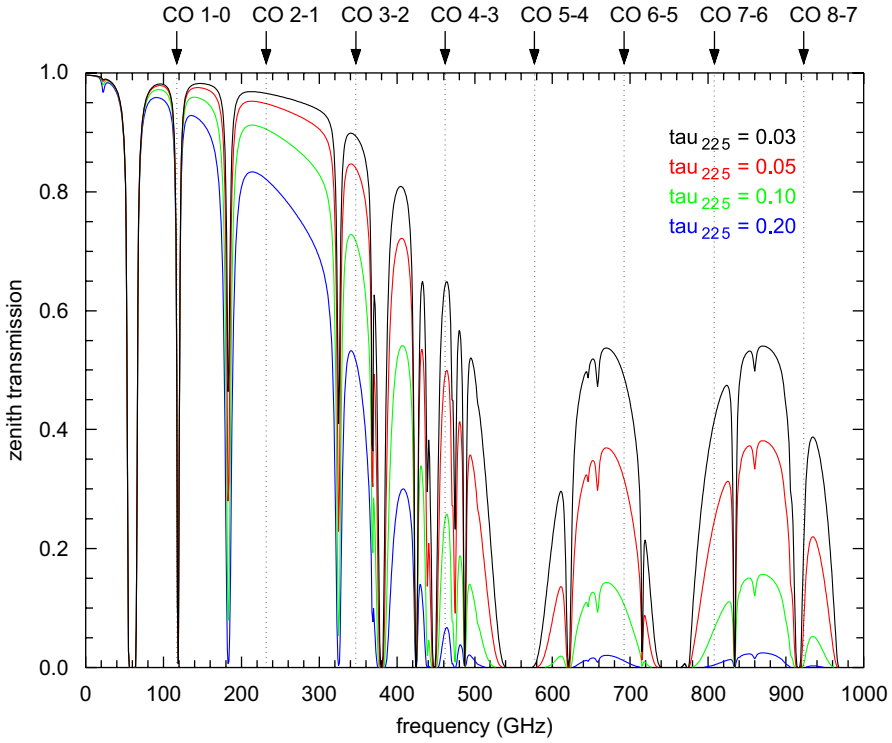

Fig. 3. Zenith transmission of the atmosphere for different 225 GHz opacities as calculated with the Microwave Propagation Model MPM93 (Liebe et al., 1993). The 225 GHz opacity has been monitored for several years at Chajnantor in the Atacama Desert, and a statistic has been compiled (Radford and Nyman, 2001). The red curve corresponds to the median of the 225 GHz opacities, and the black line to the lowest opacities.

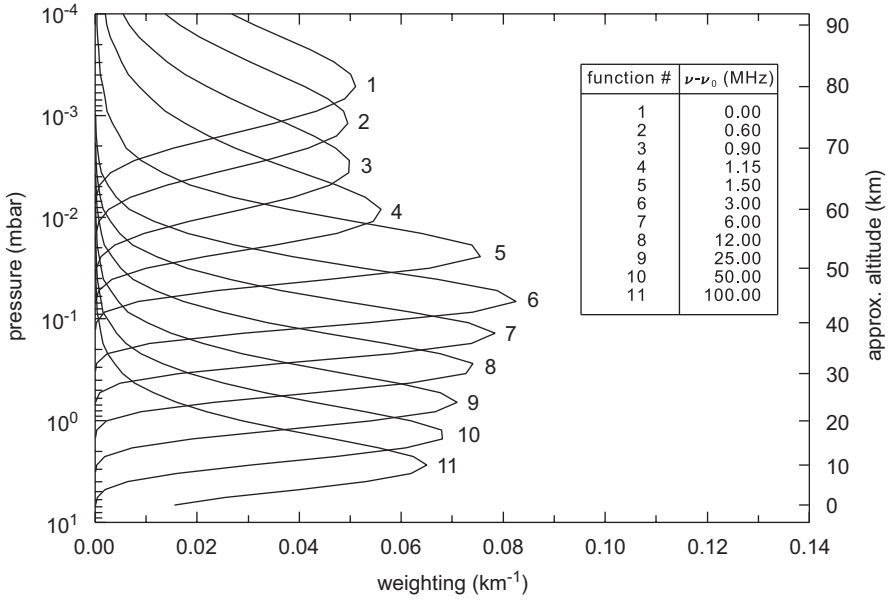

Fig. 4. Weighting functions for the CO 6-5 line in the Martian atmosphere (ground-based measurement, integrated over the whole disc with 32 rings in nadir and 32 rings covering the limb contributions). For the frequency offset zero, the weighting function peaks at 80 km.

has been proposed already in the late 1980s (Muhleman et al., 1990). Muhleman and Clancy (1995) studied a millimeter wave limb sounder for Mars and proposed it as part of the InterMarsNet mission (Taylor et al., 1996). A Martian sub-millimeter wave limb sounder (MIME) has been proposed for the first time as part of the Mars Express mission (Hartogh, 1998; Hartogh et al., 1998). A number of proposals and studies followed from which we would like to mention MAMBO (Forget et al., 2002), MARVEL (Allen et al., 2002), and, finally, SWI (de Maagt et al.,

2004). In the following section we will present results of radiative transfer and retrieval simulations of temperatures and winds performed for a sub-millimeter limb sounder. This work is related to the instrumental capabilities of MIME and SWI.

4. Retrieval simulation for a sub-millimeter limb sounder

To investigate the measurement capabilities of an orbiting sub-millimeter wave limb sounding instrument, we performed retrieval calculations for several sets of simulated model spectra. The instrumental specifications assumed for the simulation of the model spectra are as follows:

- Double sideband receiver tuned to simultaneously observe the 5–4 rotational transition of 12-CO at 576.27 GHz in one sideband and 13-CO at 550.93 GHz in the other sideband.

The reason for selecting these two lines lies in their different opacity. The idea behind this approach is to increase the "retrieval dynamic range" of the limb scan: at low pointing altitudes, the strong line becomes opaque while the weak line is still optically thin enough in the line wings. Temperature and wind information is mainly retrieved from the weak line. At high pointing altitudes the weak line disappears in the noise, while the strong line is still detectable with a reasonable SNR (Fig. 5). Simultaneous measurements of two lines with different opacity allow to retrieve temperature and volume mixing ratio of CO at the same time. The latter is required for sounding the upper part of the Martian atmosphere, since the assumption of a constant volume mixing ratio is not valid anymore.

- Four hundred MHz total spectrometer bandwidth with a frequency resolution of 100 kHz (4000 channels). The receiver is tuned in such a way that the two transitions appear separated by 100 MHz in the spectrometer.
- Circular polar orbit at 500 km altitude; side looking instrument.
- Gaussian beam pattern with a full width at half maximum (FWHM) of 0.15°, corresponding to an instrumental aperture (telescope main dish diameter) of approximately 25 cm.

In order to reduce the computational time for the retrieval calculations, the large number of equidistant spectrometer channels has been reduced by averaging channels according to their offset frequency from the line centre. Within a frequency offset of ±2 MHz, the original resolution of 100 kHz has been kept; between 2 and 6 MHz, the resolution has been reduced to 200 kHz; between 6 and 10 MHz to 500 kHz; between 10 and 14 MHz to 1000 kHz; and, finally, for offset frequencies larger than ±14 MHz, the spectral resolution of 2000 kHz has been used. In this way, the 400 MHz bandwidth of the spectrometer has been completely covered by only 380 non-uniformly distributed channels instead of the 4000 original channels.

Between the ground and 110 km, the Martian atmosphere has been described by 56 discrete layers of 2 km thickness with uniform temperature and pressure within a single layer. For this simulation, the CO volume mixing ratio has been set to constant 800 ppm, and for the 12-C/13-C isotopic ratio, a value of 90 has been used.

A full limb scan of the instrument has been simulated by calculating the set of 47 spectra for tangent altitudes between 6 and 100 km at a stepsize of 2 km. For each single spectrum, corresponding to a tangent altitude, the instrumental beam pattern has been taken into account. Finally, Gaussian noise with a standard deviation depending on each channel's bandwidth according to the radiometer formula

$$\delta T = \frac{T_n}{\sqrt{\delta t \cdot \delta v}} \tag{2}$$

has been added to the set of spectra. Here δT denotes the standard deviation, δt is the integration time for a single spectrum of the set of spectra, and δv is the bandwidth of a channel. T_n is the double sideband noise temperature of the system which has been set to 2500 K. Various integration times between 0.1 and 10 s have been tried in order to investigate the influence of the noise level on the retrieval error. Fig. 5 shows nine spectra from such a simulated limb scan with tangent altitudes between 20 an 100 km, separated by 10 km.

The measurement capabilities of the instrument have been studied by retrieving the temperature and wind profiles from such a simulated limb scan using the Optimal Estimation Technique (Rodgers, 1976). Both the temperature and the wind profile have been simultaneously retrieved from the full set of limb scanning spectra; thus the dimension of the so-called measurement vector is given by the number of channels times the number of spectra in the set, and the dimension of the profile vector is twice the number of discrete atmospheric layers, because there are two profiles to retrieve.

Essential for the application of the Optimal Estimation Technique is the description of the apriori knowledge of the profiles to be retrieved. This apriori knowledge is given in terms of a most likely profile (the so-called apriori profile) together with its uncertainty given in terms of the covariance matrix. For the apriori profile, we used the same distribution as was taken for the spectra simulation. The covariance matrix for both the temperature and wind has been chosen to be non-diagonal, specifying the correlation length of 6 km (corresponding to the footprint size of the antenna beam at the tangential heights) as described in (Rodgers, 1990, Eq. 16). The standard deviation describing the uncertainty of the apriori profile has been set to 20 K for the temperature, and to 80 m s^{-1} for the wind profile. Note that we neglect pointing errors here. Errors of the spacecraft

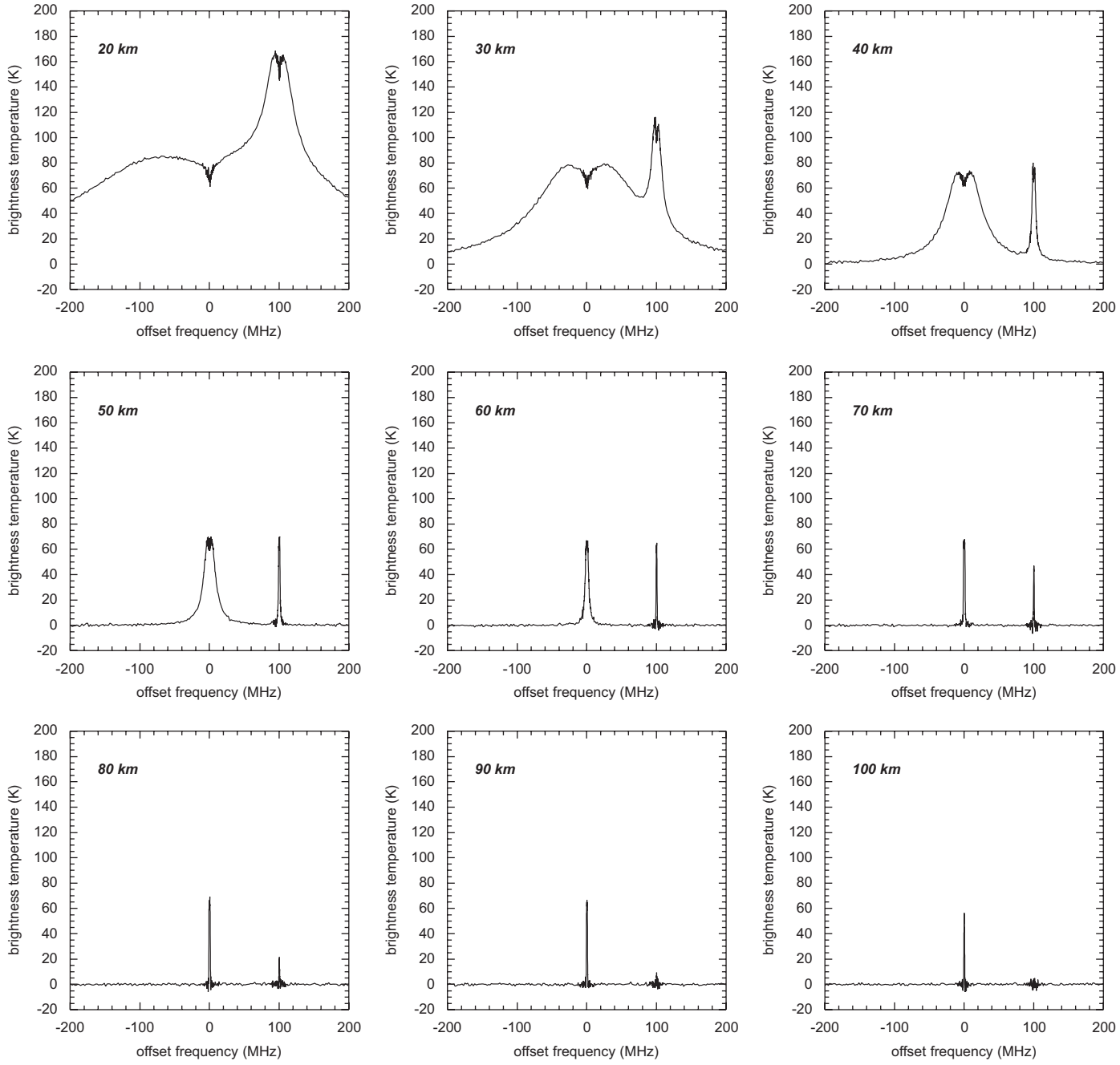

Fig. 5. Simulated limb sounding spectra of 12-CO (576 GHz) and 13-CO (551 GHz) for tangential altitudes between 20 and 100 km observed from 500 km altitude (see text).

attitude of about 1 arcmin result in wind retrieval errors of about 1 m s^{-1}.

Fig. 6 shows a typical vertical temperature distribution obtained in the simulation described above. The comparison of the vertical profile and the averaging kernels with typical ground-based results (e.g., Fig. 2) clearly shows the higher sensitivity of the limb scan, especially at altitudes above 50 km.

In this setup, after 10 s of integration time, the noise level of a 1 MHz channel is 0.79 K, which translates into a statistical wind and temperature retrieval error of about 1 to 5 K and 4 to 10 m s^{-1}, respectively, in the altitude region between 40 and 100 km. The vertical resolution of the temperature retrieval varies between 5 and 9 km, and is around 7 km for the wind retrieval (see Fig. 7). The strong increase of the wind speed error below 40 km can be explained by the decreasing brightness temperature gradient towards lower altitudes, i.e., amplitude differences caused by Doppler shifts disappear in the measurement noise. In a practical instrument we have to add the influence of systematic errors as for instance caused by reflections and non-linearities in the receiver and spectrometer subsystems. This so-called baseline ripples may cause large retrieval errors in the lower atmosphere provided they cannot be modelled.

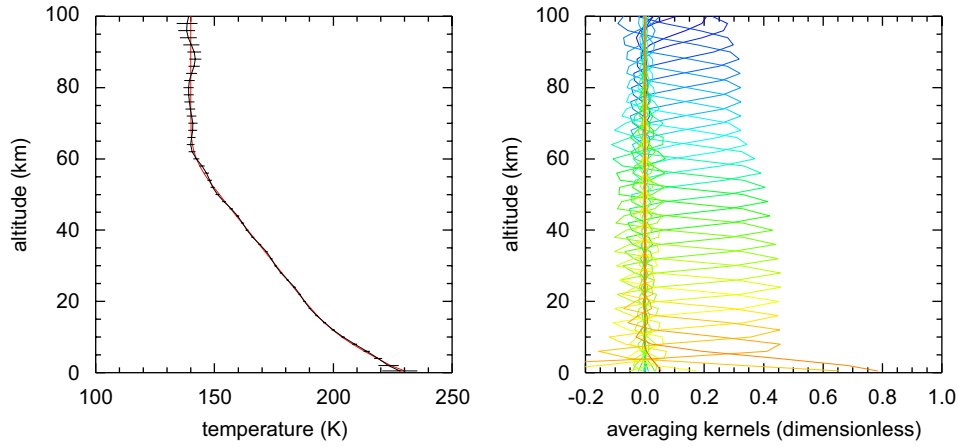

Fig. 6. Temperature limb scan retrieval simulation of the Martian atmosphere. Compare with the averaging kernel functions (a measure of the observation sensitivity to a certain altitude) of Fig. 2.

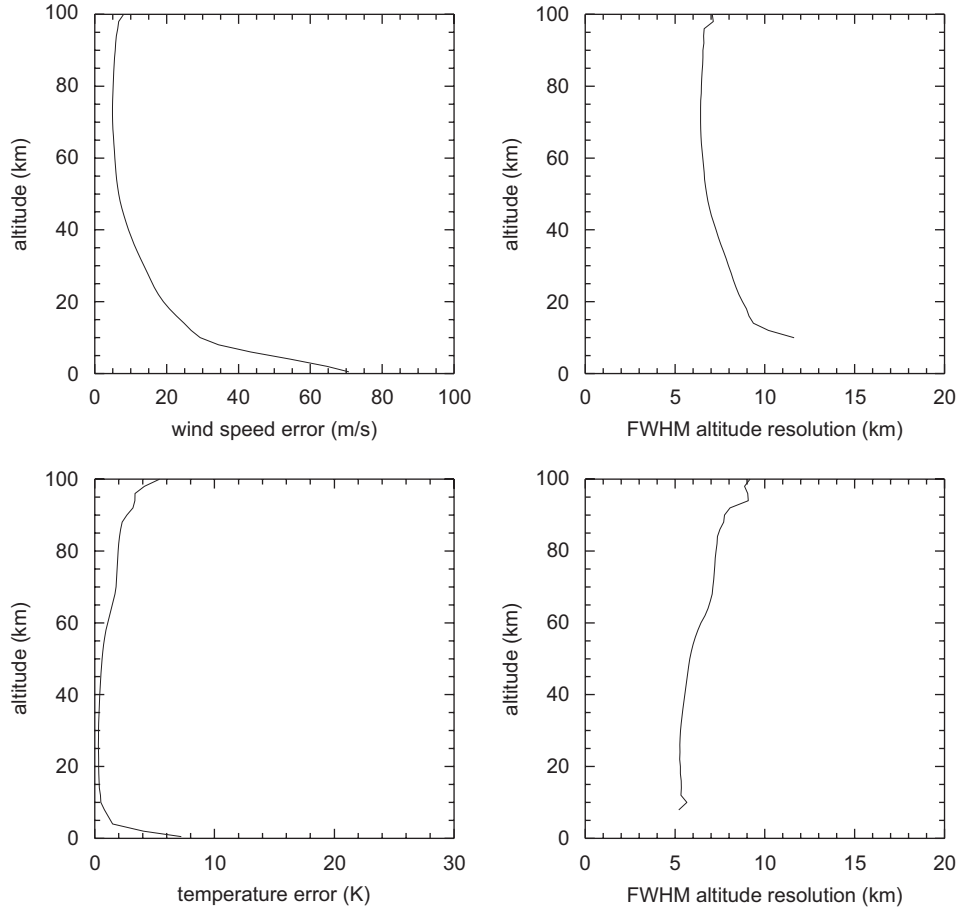

Fig. 7. Simulation of the temperature- and wind speed errors and the corresponding vertical resolution for a limb scan.

5. Summary and conclusions

Temperature inversions above 30–40 km, and the associated warmings in the Martian polar winter atmosphere are caused by the adiabatic heating due to the descending branch of the poleward Hadley circulation. Using our recently developed Martian GCM, we demonstrate that global meridional transport in the middle atmosphere of Mars is driven primarily by the eddies (planetary waves and tides) through the mechanism called "extra-tropical pump", similar to the one in the terrestrial atmosphere. Existing observations cannot definitely validate the magnitude

and location of the Martian winter polar warmings, and to constrain general circulation models. We evaluate and discuss the capabilities of ground-based observations using a sub-millimeter wave interferometer, and present radiative transfer and retrieval simulations for a low circular Mars orbit sub-mm wave limb sounder. The very good atmospheric transmission at Chajnantor (the ALMA site) will allow observations of the CO 6-5 rotational transition in the Martian atmosphere. This line can be used to retrieve wind and temperature profiles from the surface up to about 80 km and higher, depending on the solar longitude. According to the simulation results, the sub-mm limb sounder provides high quality wind and temperature data up to at least 100 km, which is very well suited for the validation of our GCM calculations.

Acknowledgements

This work was supported by Deutsche Forschungsgemeinschaft, project HA 3261/1-2.

References

Aellig, C.P., Kämpfer, N., Rudin, C., Bevilacqua, R.M., Degenhardt, W., Hartogh, P., Jarchow, C., Künzi, K., Olivero, J.J., Croskey, C., Waters, J.W., Michelsen, H.A., 1996. Latitudinal distribution of upper stratospheric ClO as derived from space borne microwave spectroscopy. Geophys. Res. Lett. 23, 2321–2324.

Allen, M., Baross, J., Chin, G., Christensen, P., Clancy, R.T., Clark, B., Drummond, J., Eiler, J., Hartogh, P., Hipkin, V., Janssen, M., Michelangeli, D., Nealson, K., Richardson, M., Rossman, G., Rye, R., Syvertson, M., Toon, G., Wennberg, P., Yunk, Y., 2002. Mars Volcanic Emission and Life Scout. A Mars Scout Proposal Submitted in response to AO 02-0SS-02.

Andrews, D.G., Holton, J.R., Leovy, C.B., 1987. Middle Atmosphere Dynamics. Academic Press, San Diego, CA.

Barnes, J.R., 1990. Possible effects of breaking gravity waves on the circulation of the middle atmosphere of Mars. J. Geophys. Res. 95 (B2), 1401–1421.

Barnes, J.R., Haberle, R.M., 1996. The Martian zonal-mean circulation: angular momentum and potential vorticity structure in GCM simulations. J. Atmos. Sci. 53, 3143–3156.

Barnes, J.R., Hollingsworth, J.L., 1987. Dynamical modeling of a planetary wave mechanism for a Martian polar warming. Icarus 71 (2), 313–334.

Christensen, P.R., Bandfield, J.L., Hamilton, V.E., Ruff, S.W., Kieffer, H.H., Titus, T.N., Malin, M.C., Morris, R.V., Lane, M.D., Clark, R.L., Jakosky, B.M., Mellon, M.T., Pearl, J.C., Conrath, B.J., Smith, M.D., Clancy, R.T., Kuzmin, R.O., Roush, T., Mehall, G.L., Gorelick, N., Bender, K., Murray, K., Dason, S., Greene, E., Silverman, S., Greenfield, M., 2001. Mars Global Surveyor Thermal Emission Spectrometer experiment: investigation description and surface science results. J. Geophys. Res 106, 23823–23872, 10.1029/2000JE001370.

Clancy, R.T., Sandor, B.J., 1998. CO_2 ice clouds in the upper atmosphere of Mars. Geophys. Res. Lett. 25 (4), 489–492.

Clancy, R.T., Muhleman, D.O., Berge, G.L., 1990. Global changes in the 0–70 km thermal structure of the Mars atmosphere derived from 1975 to 1989 microwave CO spectra. J. Geophys. Res 95, 14543–14554.

Collins, M., Lewis, S.R., Read, P.L., 1997. Gravity wave drag in a global circulation model of the Martian atmosphere: parameterization and validation. Adv. Space Res. 19 (8), 1245–1254.

Delacourt, C., Gros, N., Allemand, P., Baratoux, D., 2003. Online Mars digital elevation model derived from MOLA profiles. Eos Trans. AGU 84 (52).

Deming, D., Mumma, M.J., Espenal, F., Kostiuk, T., Zipoy, D., 1986. Polar warming in the middle atmosphere of Mars. Icarus 66, 366–379.

Forget, F., Hourdin, F., Fournier, R., Hourdin, C., Talagrand, O., Collins, M., Lewis, S.R., Read, P.L., Huot, J.-P., 1999. Improved general circulation models of the Martian atmosphere from the surface to above 80 km. J. Geophys. Res 104, 24155–24175.

Forget, F., Beaudin, G., Booth, R., Deschamps, A., Frerking, M., Frisk, U., Gheaudin, M., Gulkis, S., Hartogh, P., Janssen, M.A., Murtagh, D., Raisanen, A., Ricaud, P., Riley, L., Thomas, B., 2002. Mars Atmospheric Microwave Brightness Observer. A proposal for the scientific Payload onboard the CNES 2007 Premier orbiter.

Formisano, V., Angrilli, F., Arnold, G., Atreya, S., Bianchini, G., Biondi, D., Blanco, A., Blecka, M.I., Coradini, A., Colangeli, L., 2005. The Planetary Fourier Spectrometer (PFS) onboard the European Mars Express Mission. Planet. Space Sci. 53 (10), 959–1095.

Haberle, R.M., Pollack, J.B., Barnes, J.R., Zurek, R.W., Leovy, C.B., Murphy, J.R., Lee, H., Schaeffer, J., 1993. Mars atmospheric dynamics as simulated by NASA Ames general circulation model, 1. The zonal-mean circulation. J. Geophys. Res 98, 3093–3123.

Hartogh, P., 1998. Solar system research with microwaves. In: Attema, E., Schwehm, G., Wilson, A. (Eds.), Proceedings of the 32nd ESLAB Symposium: Remote Sensing Methodology for Earth Observation and Planetary Exploration. ESA SP-423, ESA Publ. Div., Noordwijk, pp. 23–32.

Hartogh, P., Allen, M., Beaudin, G., Calcutt, S., Chin, G., Clancy, P.T., Encrenaz, T., Forget, F., Frerking, M., Gheudin, M., Glassmeier, K.-H., Gulkis, S., Ip, W.-H., Irwin, P., Janssen, M., Jarchow, C., Keller, H.-U., Lewis, S., Mann, I., Markiewicz, W., Read, P., Riley, L., Song, L., Thomas, N., Vellacott, T., Zurek, R., 1998. Microwave Investigation on Mars Express. Proposal in response to AO ESA/SCI(97).

Hartogh, P., Medvedev, A.S., Kuroda, T., Saito, R., Villanueva, G., Feofilov, A.G., Kutepov, A.A., Berger, U., 2005. Description and climatology of a new general circulation model of the Martian atmosphere. J. Geophys. Res. 110, 10.1029/2005JE002498.

Hourdin, F., Forget, F., Talagrand, O., 1995. The sensitivity of the Martian surface pressure and atmospheric mass budget to various parameters: a comparison between numerical simulations and Viking observations. J. Geophys. Res. 100, 5501–5523.

Kakar, R.K., Walters, J.W., Wilson, W.J., 1977. Mars - Microwave detection of carbon monoxide. Science 196 (3), 1090–1091.

Kuroda, T., Hashimoto, N., Sakai, D., Takahashi, M., 2005. Simulation of the Martian atmosphere using a CCSR/NIES AGCM. J. Met. Soc. Japan 83, 1–19.

Lellouch, E., Goldstein, J.J., Bougher, S.W., Paubert, G., Rosenqvist, J., 1991. First absolute wind measurements in the middle atmosphere of Mars. Astrophys. J. 383, 401–406.

de Maagt, P., van den Berg, M., Falkner, P., Chicarro, A.F., Hartogh, P., Henderson, R., and the CDF study team, 2004. Sub-Millimeter Wave Instrument for Mars. CDF IDA Study Report, SWI, ESA-CDF-34(A).

Mellon, M.T., Jakosky, B.M., Kieffer, H.H., Christensen, P.R., 2000. High resolution thermal inertia mapping from the Mars Global Surveyor Thermal Emission Spectrometer. Icarus 148, 437–455.

Moreno, R., Guilloteau, S., Lellouch, E., Encrenaz, T., Forget, F., Chassefiere, E., Jegou, F., Hourdin, F., 2001. Mars' wind measurements at Equinox: IRAM PdB Interferometric CO observations, American Astronomical Society, DPS Meeting 33, 19.21. Bull. Am. Astron. Soc. 33, 1072.

Moudden, Y., McConnel, J.C., 2005. A new model for multiscale modeling of the Martian atmosphere, GM3. J. Geophys. Res. 110, E04001, 10.1029/2004JE002354.

Muhleman, D.O., Clancy, R.T., 1995. Microwave spectroscopy of the Mars atmosphere. Appl. Optics 34, 6067–6080.

Muhleman, D.O., Clancy, T.R., Encrenaz, T., Goldsmith, P., Grossman, A.W., Gulkis, S., Hartogh, P., Ip, W.H., Kuenzi, K., Lellouch, E.,

Marten, A., Mueller, C., Schloerb, F.P., Yung, Y.L., 1990. Microwave Spectrometer and Radiometer Experiment, Proposal to the National Aeronautics and Space Administration, Cassini Mission: Saturn Orbiter.

Plumb, R.A., 2002. Stratospheric transport. J. Meteor. Soc. Japan 80, 793–809.

Radford, S., Nyman, L.A., 2001. Site characterization. ALMA Construction Project Book (Chapter 14). 2001-07-25, ⟨http://www.alma.nrao.edu/projectbk/construction/chap14/chap14.pdf⟩.

Rodgers, C.D., 1976. Retrieval of atmospheric temperature and composition from remote measurement of thermal radiation. Rev. Geophys. Space Phys. 14, 609–624.

Rodgers, C.D., 1990. Characterization and error analysis of profiles retrieved from remote sounding. J. Geophys. Res 95, 5587–5595.

Santee, M., Crisp, D., 1993. Thermal structure and dust loading of the Martian atmosphere during late southern summer—Mariner-9 revisited. J. Geophys. Res 98 (E2), 3261–3279.

Smith, M.D., Pearl, J.C., Conrath, B.J., Christensen, P.R., 2001. Thermal Emission Spectrometer results: Mars atmospheric thermal structure and aerosol distribution. J. Geophys. Res 106, 23, 929–23, 945.

Taylor, F.W., Calcutt, S.B., Irwin, P.G.J., McCleese, D.J., Schofield, J.T., Muhleman, D.O., Clancy, R.T., Leovy, C.B., 1996. Remote sounding of the Martian atmosphere in the context of the InterMarsNet mission: general circulation and meteorology. Planet. Space Sci. 44, 1347–1360.

Theodore, B., Lellouch, E., Chassefiere, E., Hauchecorne, A., 1993. Solstial temperature inversions in the Martian middle atmosphere: observational clues and 2-D modeling. Icarus 105, 512–528.

Waters, J.W., 1993. In: Janssen, M.A. (Ed.), Microwave limb sounding, atmospheric remote sensing by microwave radiometry. Wiley, New York.

Waters, J.W., Manney, G.L., Read, W.G., Froidevaux, L., Flower, D.A., Jarnot, R.F., 1995. UARS MLS observations of lower stratospheric ClO in the 1992–93 and 1993–94 Arctic winter vortices. Geophys. Res. Lett. 22, 823–826.

Wilson, R.J., 1997. A general circulation model of the Martian polar warming. Geophys. Res. Lett. 24, 123–126.

Wilson, R.J., Hamilton, K., 1996. Comprehensive model simulation of thermal tides in the Martian atmosphere. J. Atmos. Sci 53, 1290–1326.